X-ray emission is globally correlated with massive star-forming regions, which include the Galactic Centre, Arches, and Quintuplet clusters[21]. In particular, the Quintuplet cluster is thought to be responsible for producing distinct shell-like structures as seen in radio and mid-infrared (Fig. 3). These structures, together with the enclosed diffuse X-ray-emitting materials, are probably a product of mechanical energy release from massive stars in the form of supernova explosions and fast stellar winds.

It is interesting to compare the massive star-forming regions of the Galactic Centre with the 30 Doradus nebula. The collective energy releases in the two regions are similar[21,22]. With an overall extent of about 300 pc, the 30 Dor nebula consists of 'blisters' of X-ray-emitting gas enclosed in photon-ionized loops and shells[22]. But the bulk of the X-ray emission arises in gas with a characteristic temperature $\lesssim 10^7$ K, and the gas apparently cools off with increasing distance from the central cluster R136. However, such gas in the Galactic Centre region is not traced by X-rays observed in our Chandra survey, because of the heavy foreground absorption ($\sim 10^{23}$ cm^{-2}). The strongly enhanced hard X-ray emission ($\gtrsim 4$ keV) is thus unique to the Galactic Centre environment. The expansion and outflow of the high-pressure and buoyant plasma (or cosmic rays) may be responsible for the large-scale, diffuse radio and X-ray features which are oriented perpendicularly above and below the Galactic plane and are centred on the Galactic Centre region[23,24]. □

Received 18 October; accepted 4 December 2001.

1. Koyama, K. *et al.* ASCA view of our Galactic center: Remains of past activities in X-rays? *Publ. Astron. Soc. J.* **48,** 249–255 (1996).
2. Sidoli, L. & Mereghetti, S. The X-ray diffuse emission from the Galactic center. *Astron. Astrophys.* **349,** L49–L52 (1999).
3. Valinia, A. *et al.* On the origin of the iron K line in the spectrum of the Galactic X-ray background. *Astrophys. J.* **543,** 733–739 (2000).
4. Tanaka, Y., Koyama, K., Maeda, Y. & Sonobe, T. Unusual properties of X-ray emission near the Galactic center. *Publ. Astron. Soc. J.* **52,** L25–L30 (2000).
5. Wang, Q. D., Gotthelf, E. V., Lang, C. & Jagodzinski, F. UMass/Columbia Chandra X-ray survey of the Galactic center region. *Astrophys. J.* (submitted).
6. Sidoli, L., Belloni, T. & Mereghetti, S. A catalogue of soft X-ray sources in the Galactic center region. *Astron. Astrophys.* **368,** 835–844 (2001).
7. Sakano, M. *et al.* ASCA X-ray source catalogue in the Galactic center region. *Astrophys. J. Suppl. Ser* (in the press); also as preprint astro-ph/0108376 at ⟨http://xxx.lanl.gov⟩ (2001).
8. Ebisawa, K. *et al.* Origin of the hard X-ray emission from the Galactic plane. *Science* **293,** 1633–1635 (2001).
9. Barret, D. *et al.* Hard X-ray emission from low-mass X-ray binaries. *Astrophys. J.* **533,** 329–351 (2000).
10. Feng, Y. X. *et al.* Evolution of iron Kα: Line emission in the black hole candidate GX339-4. *Astrophys. J.* **553,** 394–398 (2001).
11. Yusef-Zadeh, F. *et al.* Detection of X-ray emission from the Arches cluster near the Galactic center. *Astrophys. J.* (in the press); also as preprint astro-ph/0108174 at ⟨http://xxx.lanl.gov⟩ (2001).
12. Baganoff, F. *et al.* Rapid X-ray flaring from the direction of the supermassive black hole at the Galactic Centre. *Nature* **413,** 45–48 (2001).
13. Murakami, H., Koyama, K. & Maeda, Y. Chandra observations of diffuse X-rays from the Sagittarius B2 cloud. *Astrophys. J.* **558,** 687–692 (2001).
14. Maeda, Y. *et al.* A Chandra study of Sgr A East: A supernova remnant regulating the activity of our Galactic center? *Astrophys. J.* (in the press).
15. Jackson, J. M., Heyer, M. H., Paglione, T. & Bolatto, A. HCN and CP in the central 630 parsecs of the Galaxy. *Astrophys. J.* **456,** L91–L95 (1996).
16. Price, S. D. *et al.* Midcourse space experiment of the Galactic plane. *Astrophys. J.* **121,** 2819–2842 (2001).
17. Fromerth, M. J., Melia, F. & Leahy, D. A. A Monte Carlo study of the 6.4 keV emission at the Galactic center. *Astrophys. J.* **547,** 129–132 (2001).
18. Tsuboi, M., Ukita, N. & Handa, T. An expanding shell-like molecular cloud near the Galactic center arc. *Astrophys. J.* **481,** 263–266 (1997).
19. Yusef-Zadeh, F., Wardle, M. & Parastaran, P. The nature of the Faraday screen toward the Galactic center nonthermal filament G359.54+0.18. *Astrophys. J.* **475,** 119–122 (1997).
20. Boggs, S. E. *et al.* Diffuse galactic soft gamma ray emission. *Astrophys. J.* **544,** 320–329 (2000).
21. Figer, D. *et al.* Hubble Space Telescope/NICMOS observations of massive stellar clusters near the Galactic center. *Astrophys. J.* **525,** 750–758 (1999).
22. Wang, Q. D. Structure and evolution of hot gas in 30 Dor. *Astrophys. J.* **510,** L139–L143 (1999).
23. Almy, R. C., McCammon, D., Digel, S. W., Bronfman, L. & May, J. Distance limits on the bright X-ray emission toward the Galactic center: Evidence for a very hot interstellar medium in the Galactic X-ray bulge. *Astrophys. J.* **545,** 290–300 (2000).
24. Sofue, Y. Bipolar hypershell Galactic center starburst model: further evidence from ROSAT data and new radio and X-ray simulations. *Astrophys. J.* **540,** 224–235 (2000).
25. Townsley, L. K., Broos, P. S., Garmire, G. & Nousek, J. Mitigating charge transfer inefficiency in the Chandra X-ray observatory advanced CCD imaging spectrometer. *Astrophys. J.* **534,** L139–L142 (2000).
26. Yusef-Zadeh, F., Morris, M. & Chance, D. Large, highly organised radio structures near the galactic centre. *Nature* **310,** 557–561 (1984).

Acknowledgements

We thank F. Jagodzinski for assistance in the data calibration, and L. Townsley for helping with the CTI corrections.

Competing interests statement

The authors declare that they have no competing financial interests.

Correspondence and requests for materials should be addressed to Q.D.W. (e-mail: wqd@astro.umass.edu).

Transition-metal-based magnetic refrigerants for room-temperature applications

O. Tegus, E. Brück, K. H. J. Buschow & F. R. de Boer

Van der Waals-Zeeman Instituut, Universiteit van Amsterdam, Valckenierstraat 65, 1018 XE Amsterdam, The Netherlands

Magnetic refrigeration techniques based on the magnetocaloric effect (MCE) have recently been demonstrated as a promising alternative to conventional vapour-cycle refrigeration[1]. In a material displaying the MCE, the alignment of randomly oriented magnetic moments by an external magnetic field results in heating. This heat can then be removed from the MCE material to the ambient atmosphere by heat transfer. If the magnetic field is subsequently turned off, the magnetic moments randomize again, which leads to cooling of the material below the ambient temperature. Here we report the discovery of a large magnetic entropy change in $MnFeP_{0.45}As_{0.55}$, a material that has a Curie temperature of about 300 K and which allows magnetic refrigeration at room temperature. The magnetic entropy changes reach values of

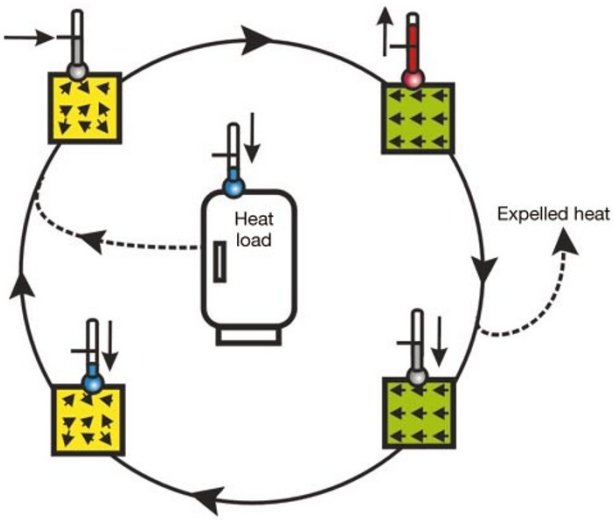

Figure 1 Schematic representation of a magnetic-refrigeration cycle, which transports heat from the heat load to its surroundings. Yellow and green depict the magnetic material in low and high magnetic fields, respectively. Initially randomly oriented magnetic moments are aligned by a magnetic field, resulting in heating of the magnetic material. This heat is removed from the material to its surroundings by a heat-transfer medium. On removing the field, the magnetic moments randomize, which leads to cooling of the magnetic material below the ambient temperature. Heat from the system to be cooled can then be extracted using a heat-transfer medium. Depending on the operating temperature, the heat-transfer medium may be water (with antifreeze) or air, and for very low temperatures, helium.

14.5 J K^{-1} kg^{-1}and 18 J K^{-1} kg^{-1} for field changes of 2 T and 5 T, respectively. The so-called giant-MCE material $Gd_5Ge_2Si_2$ (ref. 2) displays similar entropy changes, but can only be used below room temperature. The refrigerant capacity of our material is also significantly greater than that of Gd (ref. 3). The large entropy change is attributed to a field-induced first-order phase transition enhancing the effect of the applied magnetic field.

Magnetic refrigeration is an environmentally friendly cooling technology (see Fig. 1 for details). It does not use ozone-depleting chemicals (such as chlorofluorocarbons), hazardous chemicals (such as ammonia), or greenhouse gases (hydrochlorofluorocarbons and hydrofluorocarbons). Another important difference between vapour-cycle refrigerators and magnetic refrigerators is the amount of energy loss incurred during the refrigeration cycle. The cooling efficiency of magnetic refrigerators working with Gd has been shown[4] to reach 60% of the theoretical limit, compared to only about 40% in the best gas-compression refrigerators. The use of magnetic refrigerators with such high energy efficiency will result in a reduced consumption of fossil fuels, in this way contributing to a reduced CO_2 release. However, with the currently available magnetic materials, this high efficiency is only realized in high magnetic fields of 5 T. We are therefore searching for new magnetic materials displaying larger MCEs, which then can be operated in lower fields of about 2 T that can be generated by permanent magnets.

The heating and cooling that occurs in the magnetic refrigeration technique is proportional to the size of the magnetic moments and to the applied magnetic field. This is why research in magnetic refrigeration is at present almost exclusively conducted on superparamagnetic materials and on rare-earth compounds[5]. For room-temperature applications like refrigerators and air-conditioners, compounds containing manganese should be a good alternative. Manganese is a transition metal of high abundance. Also, there exist (in contrast to rare-earth compounds) an almost unlimited number of manganese compounds with magnetic ordering temperatures near room temperature. However, the magnetic moment of manganese is generally only about half that of heavy rare-earth elements. Enhancement of the caloric effects associated with magnetic moment alignment may be achieved through the induction of a first-order phase transition, which will result in much higher efficiency of the magnetic refrigerator. In combination with currently available permanent magnets, this should open the way to the development of small-scale magnetic refrigerators that no longer rely on rather costly and service-intensive superconducting magnets. Another advantage of magnetocaloric refrigerators is that the cooling power can be varied by scaling from milliwatts to a few hundred watts.

Following the discovery of a sub-room-temperature giant MCE in the ternary compound $Gd_5(Ge_{1-x}Si_x)_4$ ($0.2 \leq x \leq 0.5$), there is incentive from both fundamental and practical points of view to study the MCE in Gd-based materials[6–8]. The common feature of these compounds is that they undergo a first-order structural and magnetic phase transition, which leads to a giant magnetic-field-induced entropy change, across their ordering temperature. Many manganese compounds, such as MnAs (ref. 9), have a variety of structural and magnetic phase transitions. For a working material in a magnetic refrigerator it is, however, essential that the phase transition is also reversible. Here we report on $MnFeP_{1-x}As_x$ compounds exhibiting a large magnetic entropy change, of similar magnitude to that in the so-called giant MCE material $Gd_5Ge_2Si_2$, but whose optimum temperature of use is at and above room temperature. This result is of practical importance, because it shows that these compounds could be good working materials for magnetic refrigeration in household refrigerators or air-conditioning.

In the intermediate composition range ($0.15 \leq x \leq 0.66$), compounds in the $MnFeP_{1-x}As_x$ system crystallize in the hexagonal Fe_2P-type of structure. They have interesting magnetic properties, including a field-induced first-order magnetic transition[10]. For studying the room-temperature MCE in this system, we synthesized polycrystalline samples. The binary compounds Fe_2P and $FeAs_2$ were mixed in the appropriate proportions with Mn chips and P powder, and ground by ball milling under a protective atmosphere. The powders obtained were sealed in molybdenum tubes under an argon atmosphere, heated at 1,273 K for 120 h, followed by a homogenization process at 923 K for 120 h and finally by slow cooling to ambient conditions. The powder X-ray diffraction patterns show that the compound crystallizes in the hexagonal Fe_2P-type structure. In this structure, the Mn atoms occupy the 3(g) sites, the Fe atoms occupy the 3(f) sites and the P and the As atoms occupy 2(c) and 1(b) sites statistically[11]. From the broadening of the X-ray diffraction reflections, we estimate the average grain size to be about 100 nm.

Figure 2 shows the temperature dependence of the magnetization near room temperature of $MnFeP_{0.45}As_{0.55}$ and Gd (Alfa Aesar 3N), as determined in an applied magnetic field of 1 T. The change in magnetization in $MnFeP_{0.45}As_{0.55}$ at the ordering temperature T_C is much larger than that of Gd, despite the fact that the magnetic moment of Gd is much larger at low temperatures (248 A m^2 kg^{-1} compared to 125 A m^2 kg^{-1}). Variation of the P/As ratio between 3/2 and 1/2 makes it possible to tune T_C and the optimal operating temperature between 200 and 350 K (−70 °C and 80 °C), without losing the large MCE. Figure 2 shows magnetization measured with increasing (heating) and decreasing (cooling) temperature. The thermal hysteresis is a signature of a first-order phase transition. Because of the small size of the thermal hysteresis (less than 1 K), the

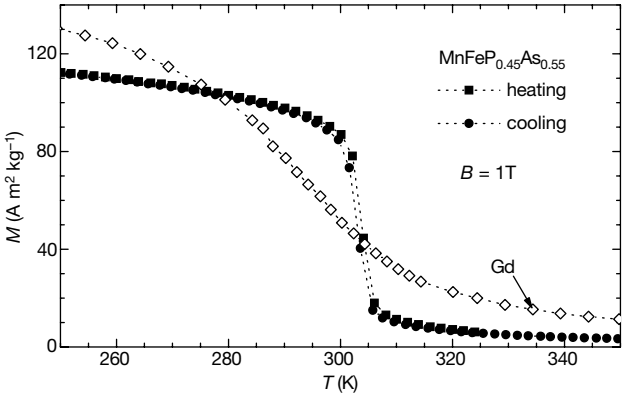

Figure 2 Temperature dependence of the magnetization M for $MnFeP_{0.45}As_{0.55}$ and Gd. Data are shown for increasing (heating) and decreasing (cooling) temperature in a field of 1 T.

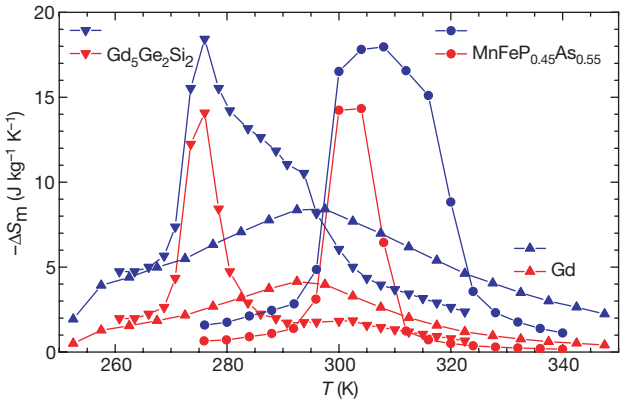

Figure 3 Magnetic entropy changes of $MnFeP_{0.45}As_{0.55}$, Gd and $Gd_5Ge_2Si_2$. Data are shown for external magnetic field changes of 0 to 2 T (red), and 0 to 5 T (blue), calculated from the magnetization data. Circles, $MnFeP_{0.45}As_{0.55}$; triangles, Gd; and inverted triangles, $Gd_5Ge_2Si_2$ (after ref. 2).

magnetization process can be considered as being reversible in temperature. From the magnetization curve at 5 K, the saturation magnetization was determined as 3.9 μ_B per formula unit. This high magnetization originates from the parallel alignment of the Mn and Fe moments, though the moments of Mn are much larger than those of Fe (ref. 12). Variation of the Mn/Fe ratio may also be used to further improve the MCE.

The magnetic entropy changes, ΔS_m, are calculated from magnetization data by means of the equation

$$\Delta S_m(T,B) = S_m(T,B) - S_m(T,0) = \int_0^B \left(\frac{\partial M}{\partial T}\right)_{B'} \mathrm{d}B'$$

which is based on a Maxwell relation. The results are shown in Fig. 3. The calculated maximum values of the magnetic entropy changes are 14.5 J kg^{-1} K^{-1} and 18 J kg^{-1} K^{-1} for field changes from 0 to 2 T and 0 to 5 T, respectively. The maximum magnetic entropy in 3*d* materials depends on the spin moment *S*. Because there are two magnetic ions per formula unit, we have $S_m = 2R\ln(2S + 1)$, where *R* is the universal gas constant. From the saturation magnetic moment, we estimate the average *S* value of the magnetic ions to be 1, thus $S_m = 18.3$ J mol^{-1} K^{-1} = 117 J kg^{-1} K^{-1}, which is about 6 times larger than the value obtained from the magnetization measurements. For comparison, the magnetic entropy change of the compound $Gd_5Ge_2Si_2$ and Gd is also shown in Fig. 3. It is evident that the MCE in $MnFeP_{1-x}As_x$ compounds is comparable with that of $Gd_5Ge_2Si_2$, though the Gd compound has a larger magnetic moment at 5 K. The origin of the large magnetic entropy change is in the comparatively high 3*d* moments and in the rapid change of magnetization in the field-induced magnetic phase transition. In rare-earth materials, the magnetic moment fully develops only at low temperatures, and therefore the entropy change near room temperature is only a fraction of the potential value. In 3*d* compounds, the strong magneto-crystalline coupling results in competing intra- and inter-atomic interactions, and leads to a modification of metal–metal distances which may change the iron and manganese magnetic moments and favour spin ordering.

The excellent magnetocaloric features of the compound $MnFeP_{0.45}As_{0.55}$, in addition to the very low material costs, make it an attractive candidate material for a commercial magnetic refrigerator. □

Received 30 July; accepted 6 November 2001.

1. Glanz, J. Making a bigger chill with magnets. *Science* **279,** 2045 (1998).
2. Pecharsky, V. K. & Gschneidner, K. A. Jr Giant magnetocaloric effect in $Gd_5(Si_2Ge_2)$. *Phys. Rev. Lett.* **78,** 4494–4497 (1997).
3. Gschneidner, K. A. Jr *et al.* Recent developments in magnetic refrigeration. *Mater. Sci. Forum* **315–317,** 69–76 (1999).
4. Zimm, C. *et al.* Description and performance of a near-room temperature magnetic refrigerator. *Adv. Cryogen. Eng.* **43,** 1759–1766 (1998).
5. Tishin, A. M. in *Handbook of Magnetic Materials* Vol. 12 (ed. Buschow, K. H. J.) 395–524 (North Holland, Amsterdam, 1999).
6. Choe, W. *et al.* Making and breaking covalent bonds across the magnetic transition in the giant magnetocaloric material $Gd_5(Si_2Ge_2)$. *Phys. Rev. Lett.* **84,** 4617–4620 (2000).
7. Giguere, A. *et al.* Direct measurement of the "giant" adiabatic temperature change in $Gd_5(Si_2Ge_2)$. *Phys. Rev. Lett.* **83,** 2262–2265 (1999).
8. Morellon, L. *et al.* Nature of the first-order antiferromagnetic-ferromagnetic transition in the Ge-rich magnetocaloric compounds $Gd_5(Si_xGe_{1-x})_4$. *Phys. Rev. B* **62,** 1022–1026 (2000).
9. Pytlik, L. & Zieba, A. Magnetic phase diagram of MnAs. *J. Magn. Magn. Mater.* **51,** 199–210 (1985).
10. Zach, R., Guillot, M. & Fruchart, R. The influence of high magnetic fields on the first order magneto-elastic transition in $MnFe(P_{1-y}As_y)$ systems. *J. Magn. Magn. Mater.* **89,** 221–228 (1990).
11. Bacmann, M. *et al.* Magnetoelastic transition and antiferro-ferromagnetic ordering in the system $MnFeP_{1-y}As_y$. *J. Magn. Magn. Mater.* **134,** 59–67 (1994).
12. Beckman, O. & Lundgren, L. in *Handbook of Magnetic Materials* (ed. Buschow, K. H. J.) Vol. 6, 181–287 (North Holland, Amsterdam, 1991).

Acknowledgements

We thank A.J. Riemersma for preparation of graphs. Part of this work was performed within the scientific exchange program between the Netherlands and China. This work was financially supported by the Dutch Technology Foundation STW.

Correspondence and requests for materials should be addressed to E.B. (e-mail: bruck@wins.uva.nl).

Remote electronic control of DNA hybridization through inductive coupling to an attached metal nanocrystal antenna

Kimberly Hamad-Schifferli*, John J. Schwartz†, Aaron T. Santos*, Shuguang Zhang‡ & Joseph M. Jacobson*

* *The Media Laboratory and the ‡Center for Biomedical Engineering, Massachusetts Institute of Technology, 77 Massachusetts Ave., Cambridge, Massachusetts 02139, USA*
† *Engeneos, 40 Bear Hill Road, Waltham, Massachusetts 02451, USA*

Increasingly detailed structural[1] and dynamic[2,3] studies are highlighting the precision with which biomolecules execute often complex tasks at the molecular scale. The efficiency and versatility of these processes have inspired many attempts to mimic or harness them. To date, biomolecules have been used to perform computational operations[4] and actuation[5], to construct artificial transcriptional loops that behave like simple circuit elements[6,7] and to direct the assembly of nanocrystals[8]. Further development of these approaches requires new tools for the physical and chemical manipulation of biological systems. Biomolecular activity has been triggered optically through the use of chromophores[9–14], but direct electronic control over biomolecular 'machinery' in a specific and fully reversible manner has not yet been achieved. Here we demonstrate remote electronic control over the hybridization behaviour of DNA molecules, by inductive coupling of a radio-frequency magnetic field to a metal nanocrystal covalently linked to DNA[15]. Inductive coupling to the nanocrystal increases the local temperature of the bound DNA, thereby inducing denaturation while leaving surrounding molecules relatively unaffected. Moreover, because dissolved biomolecules dissipate heat in less than 50 picoseconds (ref. 16), the switching is fully reversible. Inductive heating of macroscopic samples is widely used[17–19], but the present approach should allow extension of this concept to the control of hybridization and thus of a broad range of biological functions on the molecular scale.

Inductive coupling is the transfer of energy between circuits. If the secondary circuit has finite impedance, eddy currents are produced which are converted to heat by the Joule effect[17]. Heating a conductor by placing it in an alternating magnetic field is generally used to heat macroscopic samples. Here we apply it to metallic nanocrystals (diameter 1.4 nm) in solution. Induction heating is accompanied by a skin-depth effect, resulting from partial cancellation of the magnetic fields. Consequently, most of the power absorbed by the conductor is concentrated in a depth d_0, given by:

$$d_0 = \frac{1}{2\pi}\sqrt{\frac{\rho 10^7}{\mu_r \mu_0 f}} \quad (1)$$

where μ_r is magnetic permeability, μ_0 is the permeability of free space, ρ is the material resistivity, and f is the frequency of the alternating magnetic field. The power density P is given by:

$$P = 4\pi H_e^2 \mu_0 \mu_r f F \frac{d_0}{d} \quad (2)$$

where d is the sample diameter, H_e is the magnetic field strength, and F is a transmission factor that has a sigmoidal dependence on d/d_0. Optimal power absorption and heating occur when $d/d_0 = 3.5$. To optimally heat by induction a gold nanocrystal with $d = 1.4$ nm, $f = 49$ GHz (radio frequency range) is required[17,18]. Here we use